



OPEN Dosimetric and radiobiological evaluation of stereotactic radiosurgery using volumetric modulated arc therapy and dynamic conformal arc therapy for multiple brain metastases

Chen-Jun Jiang¹✉, Yick-Wing Ho², Ka-Hei Lok², Yeow-Yuen Lu⁴, Chun-Ran Zhu³✉ & Harry Chi-Yuen Cheng²✉

This paper presents a clinical comparison of the target dose, normal tissue complication probability (NTCP), and plan quality between volumetric modulated conformal arc therapy (VMAT) against dynamic conformal arc therapy (DCAT) techniques to facilitate clinical decision-making in multiple brain metastases (MBM) treatment. A total of 11 cases having 33 lesions were recruited at the Union Oncology Centre, Union Hospital, Hong Kong SAR. With CT images available, all plans were optimized using both HyperArc (HA) and Brainlab Elements Multiple Brain Metastases (Elements MBM). Target coverage, normal tissue sparing, and dose distribution were compared pairwise between VMAT and DCAT. Results showed that the plans generated using both techniques achieved adequate target coverage to meet up with the oncologist's prescription. With similar levels of NTCP, the normal brain received low doses of radiation using both techniques and the risk of brain necrosis was kept equally low. This indicated that VMAT and DCAT produced similar high-quality treatment plans with low risks of brain necrosis. Meanwhile, VMAT showed better homogeneity which could potentially be more useful for large targets, while DCAT showed better target conformity especially for targets smaller than 1 cc. In general, both HA and Elements MBM demonstrated ability to generate high-quality clinical plans.

Keywords Multiple brain metastases, Frameless stereotactic radiosurgery, VMAT, DCAT, Radiation-induced brain necrosis, NTCP, Dose distribution, Quality of life

Multiple brain metastases (MBM), affecting 8–10% of metastatic cancer patients¹, primarily originate from the intravasation of tumors in the lung (19.9%), melanoma (6.9%), or breast (5.1%), followed by extravasation in the brain area². Whole-brain radiation therapy (WBRT), as a traditional method of MBM treatment³, although effective at intracerebral control of MBM, can result in toxicity due to its indiscriminate impact on healthy brain tissue. Damage to the normal brain region could result in serious impairments to neurocognitive function (NCF), impacting the quality of life (QoL)^{4–6}. In response, stereotactic radiosurgery (SRS) has emerged as an advanced treatment of MBM in a high-dose single fraction with enhanced precision and superior local focus, reducing the impairment to NCF⁴. When it comes to MBM treatment, traditional multiple-isocenter or non-isocenter SRS planning approaches such as GammaKnife (GK) and CyberKnife (CK) have the disadvantage of time consuming, for the addition of each isocenter extends the treatment delivery by around 10 min and requires

¹Department of Diagnostic Radiology, LKS Faculty of Medicine, The University of Hong Kong, Hong Kong Island, Hong Kong SAR, China. ²The Union Oncology Centre, Kowloon, Hong Kong SAR, China. ³The Affiliated Hospital of Integrated Traditional Chinese and Western Medicine, Nanjing University of Chinese Medicine, Nanjing 210028, Jiangsu, China. ⁴The Prince of Wales Hospital, New Territories, Hong Kong SAR, China. ✉email: jche920@connect.hku.hk; zhuchunran2020@163.com; chenghcy@union.org

repeated patient positioning during treatment^{7,8}. This makes single-isocenter non-coplanar SRS techniques a more favourable option.

Linear accelerators (LINACs) were developed with SRS techniques that allows immobilization and localization without the use of invasive frames to improve treatment experience. Non-coplanar SRS has outperformed its coplanar counterpart by using multiple beams directed at flexible planes, such that the beams can converge at various angles to avoid overlapping at non-tumor regions⁹. This feature has been shown to provide increased conformity and complexity in treatment geometry, enhancing the sparing of organs at risk (OAR) and reducing the dose to normal brain tissue¹⁰, which is particularly important for high fractional treatment such as SRS. Two promising techniques that exemplify this are dynamic conformal arc therapy (DCAT) and volumetric modulated arc therapy (VMAT), both delivered by multileaf collimator (MLC) based LINACs. VMAT features dynamic modulation of MLC movement and gantry rotation speed, allowing for greater degrees of freedom. It has been suggested that VMAT produces a steep dose gradient beyond the target region, which facilitates sufficient sparing of OAR¹¹. Meanwhile, DCAT typically involves less MLC modulation but offers advantages such as a reduced calculation burden, fewer monitor units (MU), and shorter treatment times^{11,12}. Commercially available treatment planning systems (TPS) based on VMAT and DCAT are Varian HyperArc (HA) and Brainlab Elements Multiple Brain Mets (Elements MBM), respectively. To achieve a given clinical goal using VMAT and DCAT embedded TPS, competitive plans can be generated for the same patient from different solutions with different dose distributions¹¹. The variation in dose distribution can be quantified by the Conformity Index (CI) that attributes a score to measure the fitting between the prescription isodose volume and the target volume, the Gradient Index (GI) that shows the rapidness of dose decline beyond the target, and the Homogeneity Index (HI) that accounts for the uniformity of dose distribution in the target volume^{12–14}.

A common brain toxicity endpoint reported in the literature is radiation-induced brain necrosis, or radionecrosis, a result of inflammation caused by neuron cell death after SRS at the original tumor site¹⁵ which can lead to long-term complications such as headache, nausea, ataxia, and seizure^{16–18}. The incorporation of Normal Tissue Complication Probability (NTCP) model has been recommended in evaluating the risk of radionecrosis following SRS-treated MBM¹⁹. Over the past decades, different NTCP models were developed to evaluate the control ability of SRS for radionecrosis^{19–22}. Since 1997, when Niemierko introduced the concept of equivalent uniform dose (EUD) which is defined as the amount of dose that leads to the same fraction of cell survival when uniform irradiation is assumed²³, an EUD-based NTCP model was proposed compliant with the empirical normal tissue tolerance parameters developed by Emami²⁴.

Intrinsically, VMAT or DCAT techniques present differences in plan quality. It is important to understand the potential differences in treatment outcomes between the techniques for clinical decision-making. However, the few existing clinical comparison studies involving VMAT and DCAT techniques have yielded different results in terms of dosimetric characteristic and normal tissue protection ability^{25–30}. Moreover, there is a lack of clinical comparison studies using NTCP models to predict the risk of radionecrosis in SRS treatment of MBM. In this study, MBM cases treated at the Union Oncology Centre, Union Hospital, Hong Kong SAR, were retrospectively viewed. The dosimetric and radiobiological characteristics of VMAT-based HA and DCAT-based Elements MBM were compared in terms of target coverage, EUD-based NTCP, whole brain and normal brain dose, and dose distribution indices.

Methods and materials

Case recruitment

MBM cases that received SRS treatment between November 2022 and April 2024 at the Union Oncology Centre, Union Hospital, Hong Kong SAR, were included in this study. Computed tomography (CT) images of recruited patients were retrospectively viewed and were used for treatment plan generation. Due to the retrospective nature of the study, the Ethics Committee of the Union Hospital waived the need to obtain informed consent. The experimental protocol was approved by the Union Oncology Centre, Union Hospital. All research protocols were carried out under the institutional guidelines and regulations of the Union Oncology Centre, Union Hospital.

Inclusion Criteria.

- MBM cases prescribed with single fraction SRS.
- Having clinically approved prescription and treatment plans.
- Having more than one treated target.

Treatment plan generation

For each patient with a given prescription, two simulation plans were generated using two advanced single-isocenter frameless SRS techniques: Varian HyperArc (Eclipse v16.1, Varian Medical Systems, Netherlands) employing VMAT technique and Brainlab Elements MBM (Brainlab Elements v4.0, Munich, Germany) employing DCAT technique. The targets and OAR were contoured by an oncologist experienced in intracranial metastases treatment. The photon beam energy of flattening filter free (FFF, 6-MV) was used, and the LINAC type was Varian Edge. The leaf pattern for the MLC was HD120 with a central leaf thickness of 1.25 mm stepping to 2.5 mm at isocenter, and a peripheral leaf thickness of 2.5 mm stepping to 5 mm at isocenter. For both TPS, the prescription dose was given at the 80% isodose line to achieve full coverage of the gross tumor volume (GTV) and 99.5% coverage of the planning target volume (PTV); the clinical goal was set to achieve a maximum dose not exceeding 130% prescription dose, while the dose to the OAR and healthy brain was minimized. All plans were mutually evaluated and verified by the oncologist team.

HA external beam planning was conducted in Eclipse utilizing analytic anisotropic algorithm (AAA) with a calculation voxel size of 1 mm. The SRS support structure model Encompass was to match the immobilization

device. PTVs were set to high resolution structures in contouring. Partial arc treatment was utilized when the isocenter was located outside the patient protection zone, while full arc treatment was utilized if it was located inside. Normal tissue objective value was optimized to protect critical structures. All doses were corrected for heterogeneity on the 1.25 mm grid size. Figure 1 shows an example of a plan generated on HA.

Elements MBM was calculated with Pencil Beam followed by Monte Carlo algorithm with a calculation voxel size of 1 mm, following that of HA. A tissue model was generated for each case under Couch Top of Frameless Extension. For the gantry and table optimization protocol, a maximum of 2 passes and 4 extra arcs were allowed. A minimum of 4 table angles were assigned, with a maximum of 5 table angles allowed. Automatic Arc Setup Mirroring, Automatic Table Angle Optimization, and Automatic Gantry Angle Optimization were enabled for greater flexibility. Figure 2 shows an example of a plan generated on Brainlab Elements MBM.

Evaluation of indicators of target dose and whole brain dose constraints

To estimate the target dose coverage and quality of treatment of VMAT and DCAT, near-minimum dose, median dose, and near-maximum dose to each PTV (D98%, D50%, and D2%) were calculated and compared between the two systems. Based on the dose-volume constraints guided by UK consensus³¹, the whole brain volume that received 12 Gy or higher radiation (V12Gy) was recorded for each case to reflect the risk of radiation-induced toxicity to the whole brain. V10Gy, V8Gy, and V5Gy were also included to stay in line with previous studies^{25–30}. For the normal brain (brain excluding GTV), the mean dose, the volume receiving more than 12 Gy and more than 80%, 50% and 10% of the prescription dose (V12Gy, V80%, V50%, V10%) were evaluated. Following the UK consensus³¹, mean dose to the cochlea and maximum doses to the OAR including the lenses, eyes, inner ear, pituitary gland, optic nerve, optic chiasm, brainstem, and spinal cord were evaluated.

Computing indicators of dose distribution

The following indicators accounting for the dose distribution of the treatment systems were analyzed per PTV across all patient plans: Paddick Conformity Index (CI)³², RTOG CI³³, Gradient Index (GI)³⁴, RTOG Homogeneity Index (HI)³⁵, and ICRU83 HI³⁵. The equations (Eqs. 1–5) calculating the dose distribution indicators can be found in the Appendix.

Computing the NTCP model outcome

The NTCP model proposed by Niemierko was employed with the organ at risk being the healthy brain and the endpoint being radionecrosis³⁶:

$$NTCP = \frac{1}{1 + \left(\frac{EUD_{50}}{EUD} \right)^4 \gamma_{50}} \quad (1)$$

where γ_{50} describes the slope of the NTCP curve parameter, EUD_{50} stands for the dose for a 50% complication probability, and the plan specific equivalent uniform dose EUD is given by:

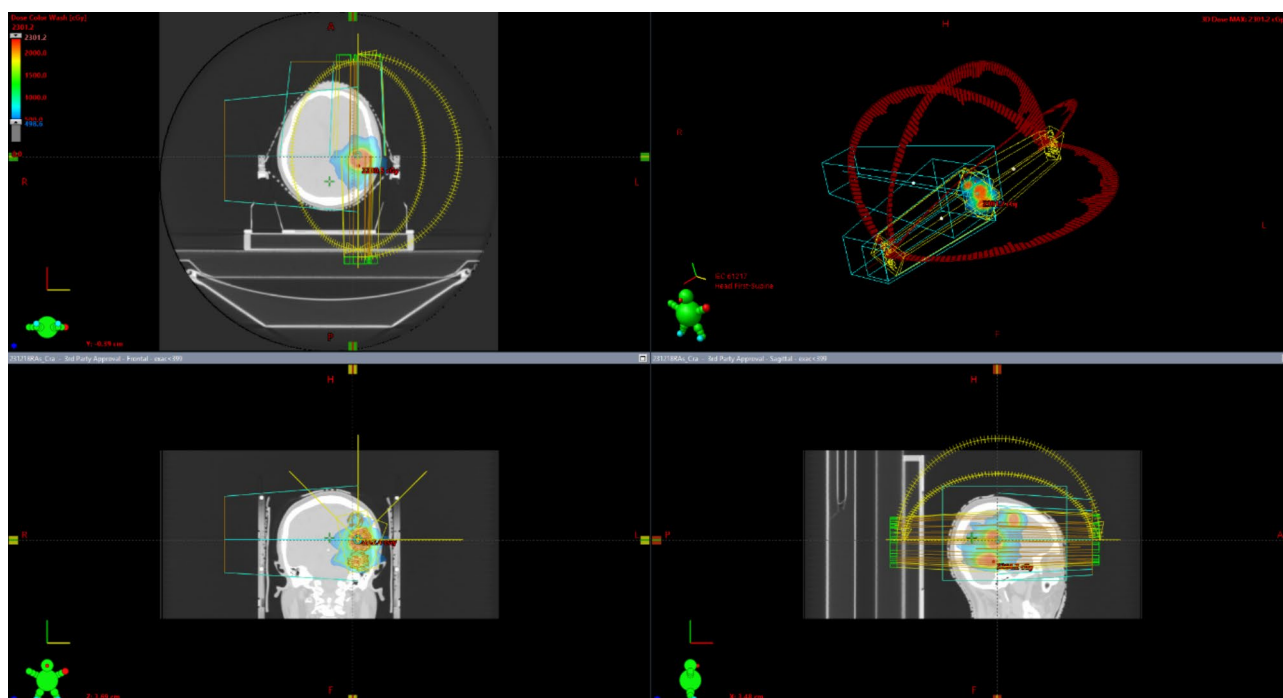


Fig. 1. HA plan preview.

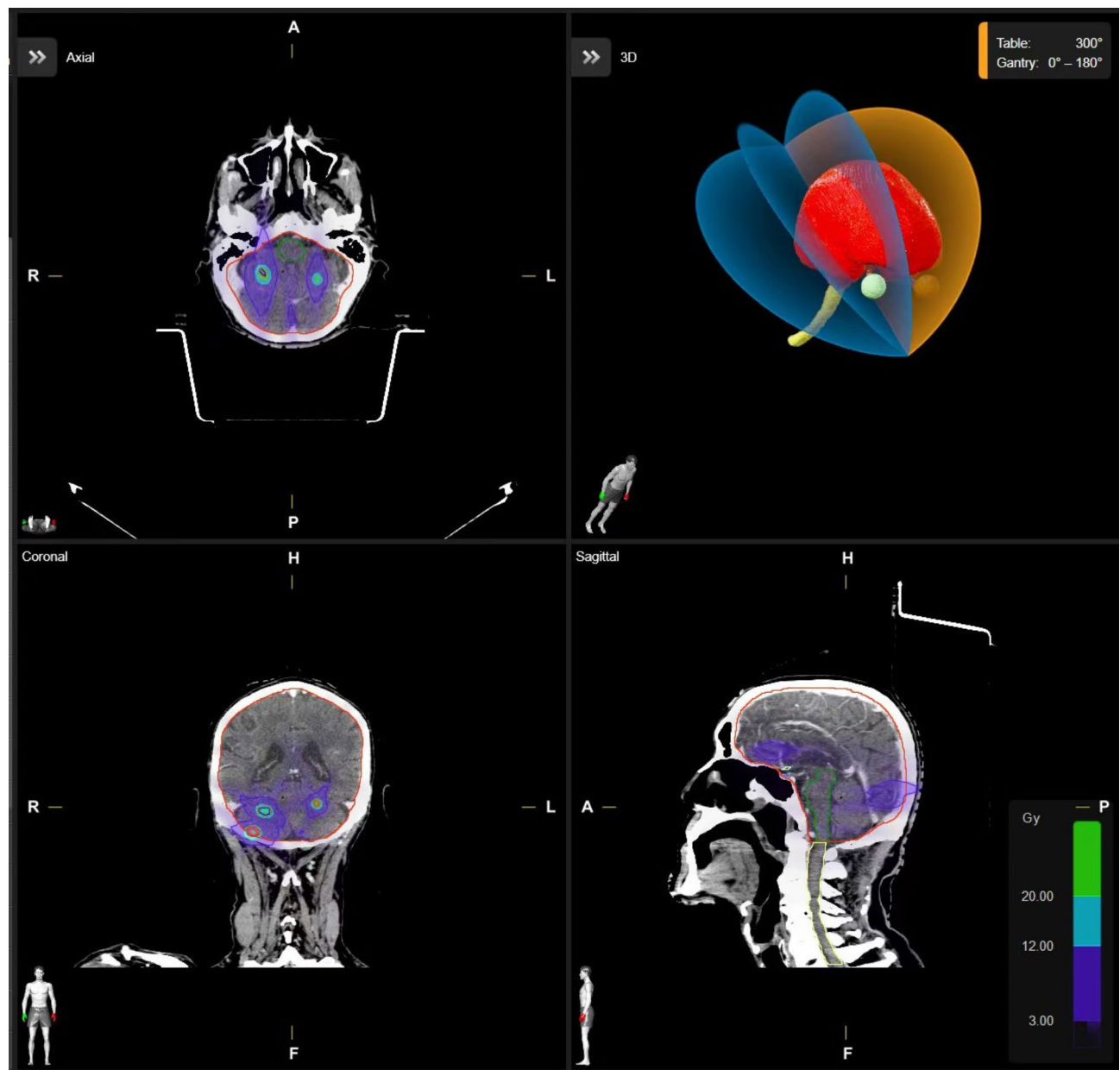


Fig. 2. Elements MBM plan preview.

$$EUD = \left(\sum_i v_i D_i^a \right)^{\frac{1}{a}} \quad (2)$$

where v_i is the partial volume with corresponding biologically equivalent absorbed dose D_i , and a is a tissue-specific fitting parameter. D_i was obtained from the differential dose-volume histogram (dDVH) using²²:

$$D_i = d_i \times \frac{\left(\frac{\alpha}{\beta} + \frac{d_i}{n_f} \right)}{\left(\frac{\alpha}{\beta} + D \right)} \quad (3)$$

where d_i is the fractional dose corresponding to the i_{th} partial volume v_i on the dDVH, α/β is a fitting parameter of the linear quadratic model of cell survival, n_f is the number of fractions prescribed, with $n_f = 1$ for single-fraction SRS, and D is the dose prescribed per fraction.

Parametrizing the above logistic NTCP function, where $EUD_{50} = 57.7 \text{ Gy}$, $\gamma_{50} = 2.5$, $\alpha/\beta = 2$, and $a = 9$ as recommended by Emami³⁷, Burman³⁸, and Niemierko et al.³⁹ that are specific to intracranial normal tissue, the NTCP model equation reduced to:

$$NTCP = \frac{1}{1 + \left(\frac{57.7}{EUD}\right)^{10}} \tag{4}$$

Where:

$$EUD = \left(\sum_i v_i D_i^9\right)^{\frac{1}{9}} \tag{5}$$

The NTCP model was developed on Excel sheets for data processing. The dDVH of the simulated plan was downloaded and input into the NTCP model. NTCP in percentage form was recorded.

Statistical analysis

Data analysis was conducted using SPSS (version 29.0.1, IBM Corp, Armonk, New York, US). Normality test was conducted for all sets of data utilizing Shapiro-Wilk (SW) test. Treatment plans simulated by VMAT and DCAT were compared pairwise. Normal distribution was satisfied if *p*-value > 0.05 in the SW test. Otherwise, normal distribution was considered violated. Normally distributed data sets were compared using the Paired Samples T Test and non-normally distributed data sets were compared using a paired Wilcoxon Signed Rank Test (WSRT) to identify differences, with two-tailed *p*-value < 0.05 considered statistically significant.

Results

A total number of 33 targets from 11 MBM cases treated with SRS between November 2022 and April 2024 were studied. The average individual volume of PTV was 1.76 cc, and the average volume of total PTV was 5.29 cc per patient. The ages ranged from 38 to 68 years old, and the mean age was 63 years old. Among these cases, 6 were females and 5 were males, with the prescription dose ranging from 18 to 24 Gy and the treatment percentage prescribed at 80% isodose line. Patient characteristics are summarized in Table 1.

Both Elements MBM and HA software achieved excellent plan dosimetry and conformity. Table 2 summarizes the median of doses received by 98%, 50%, and 20% of the target volume. The median value of the near minimum dose (D98%) was found to be higher in VMAT plans at 21.10 Gy (range 18.74–25.95 Gy), equivalent to 105.25% (range 100.01–108.10%) of the prescribed dose. However, the near-maximum doses (D2%) and doses to 50% of the target volume (D50%) were found lower in VMAT than in DCAT at 123.09% (range 119.03–128.61%) versus 124.76% (range 122.19–127.41%), and 115.64% (range 111.80–119.40%) versus 116.61% (range 112.88–120.76%).

V5Gy, V12Gy, and the maximum dose received by the whole brain are shown in Table 3. V12Gy and V5Gy for the whole brain also showed no significant difference for the two systems. The average V12Gy and V5Gy were 13.97 cc (range 2.80–61.16 cc) and 54.09 cc (range 13.60–220.38 cc) versus 13.82 cc (range 1.56–68.57 cc) and 48.51 cc (range 6.14– 235.03 cc) for VMAT and DCAT plans, respectively.

Table 4 summarizes the NTCP, and the doses received by the normal brain region excluding GTV. The average mean doses to the normal brain (brain volume excluding GTV) were similar at 1.31 ± 0.77 Gy for VMAT and 1.12 ± 0.81 Gy for DCAT. Volumes of the brain excluding GTV receiving 80%, 50%, and 10% of the prescription dose were higher for VMAT than for DCAT. A similar V12Gy was observed for the two TPS at 11.51 Gy (range 2.80–42.89 Gy) and 11.44 Gy (range 1.56–50.48 Gy), respectively. Out of 11 patients, 8 showed higher V80% and 10 showed higher V50% for VMAT plans (5.90 Gy, range 0.35–31.1 Gy) than for DCA plans (3.59 Gy, range 0.26–15.91 Gy). All 11 patients had a higher V10% for VMAT plans at 187.25 Gy (range 34.34–586.68 Gy) than for DCAT plans (range 14.23–503.86 Gy).

Patient number	Gender	Age	Prescription dose (Gy)	Treatment percentage (%)	Fraction number	Number of PTV	Total PTV volume (cc)
1	F	38	22	80	1	3	1.66
2	M	79	20	80	1	5	2.84
3	M	65	24	80	1	3	3.08
4	F	66	18	80	1	4	3.18
5	M	68	20	80	1	2	4.72
6	F	65	18	80	1	2	1.77
7	F	59	24	80	1	2	5.32
8	F	38	22	80	1	3	1.67
9	M	54	20	80	1	2	1.15
10	F	64	18	80	1	3	32.62
11	M	65	24	80	1	4	0.21
Mean		63	21			3	5.29
Range		38–68	18–24			2–5	
SD [†]		13	3				

Table 1. Patient summary. [†]SD: Standard Deviation.

PTV	Technique	Median	Mean	Range	Higher Ranks [†]	2-tailed <i>p</i> -value	Z score
D98%(Gy)	VMAT	21.10	21.88	18.74–25.95	23	<0.01	-2.91
	DCAT	21.31	21.75	18.74–25.22	10		
D50%(Gy)	VMAT	23.06	24.00	20.78–28.66	11	<0.01	-2.83
	DCAT	24.00	24.44	20.80–28.54	22		
D2%(Gy)	VMAT	24.39	25.52	21.81–30.87	10	<0.01	-3.17
	DCAT	25.31	26.06	22.19–30.35	23		
D98%(%)	VMAT	105.25	104.75	100.01–108.10	23	<0.01	-2.90
	DCAT	103.97	104.08	100.90–108.63	10		
D50%(%)	VMAT	115.64	111.38	111.80–119.40	11	<0.01	-2.97
	DCAT	116.61	116.97	112.88–120.76	22		
D2%(%)	VMAT	123.09	122.06	115.20–128.61	10	<0.01	-3.28
	DCAT	124.76	124.64	122.19–127.41	23		

Table 2. Summary of doses received by 98%, 50%, and 20% of the target volume (D98%, D50%, and D2%).

[†]Higher ranks: the number of treated target presenting greater values of D98% / D50% / D2%. (Example: Higher ranks = 23 for VMAT D98%(Gy), indicating 23 treated PTV of VMAT plans received a greater D98%(Gy) value than their Elements MBM counterparts.)

Whole brain	Technique	Median	Mean	Range	Higher ranks [†]	2-tailed <i>p</i> -value	Z score
V12Gy(cc)	VMAT	9.27	13.97	2.80–61.16	5	0.93	-0.08
	DCAT	8.65	13.82	1.56–68.58	6		
V10Gy(cc)	VMAT	12.49	18.06	3.91–76.58	5	1.00	0.01
	DCAT	11.39	18.10	2.11–89.71	6		
V8Gy(cc)	VMAT	18.78	25.60	5.83–108.50	5	0.93	0.09
	DCAT	15.94	25.11	3.02–124.82	6		
V5Gy(cc)	VMAT	36.75	54.09	13.60–220.38	6	0.42	-0.80
	DCAT	31.85	48.51	6.41–235.03	5		

Table 3. Summary of V12Gy (cc), V10Gy(cc), V8Gy(cc), and V5Gy (cc) of the whole brain. [†]Higher ranks: plans presenting greater values of V12Gy / V10Gy / V8Gy / V5Gy. (Example: Higher ranks = 5 for VMAT V12Gy(cc), indicating 5 VMAT plans had a greater whole brain V12Gy value than their Elements MBM counterparts.)

Normal brain	Technique	Median	Mean	Range	Superior Plans [†]	2-tailed <i>p</i> -value	Z score
NTCP (%)	VMAT	0.13%	0.67%	0.01–4.39%	7	0.72	-0.36
	DCAT	0.11%	0.35%	0.02–1.09%	4		
					Higher Ranks [‡]		
Mean Dose (Gy)	VMAT	1.23	1.31	0.64–3.13	8	0.750	-1.78
	DCAT	1.02	1.12	0.36–3.38	3		
V12Gy (cc)	VMAT	8.59	11.51	2.80–42.89	5	0.930	-0.08
	DCAT	7.61	11.44	1.56–50.48	6		
V80% (cc)	VMAT	3.11	5.90	0.35–31.10	8	<0.05	-2.22
	DCAT	2.76	3.59	0.26–15.91	3		
V50% (cc)	VMAT	8.54	14.29	1.79–71.37	10	<0.01	-2.58
	DCAT	7.89	10.44	0.99–51.50	1		
V10% (cc)	VMAT	107.00	187.25	34.34–586.68	11	<0.01	-2.93
	DCAT	80.56	117.28	14.23–503.86	0		

Table 4. Doses to the normal brain and NTCP scores. [†]Superior plans: plans having lower NTCP values. [‡]Higher ranks: plans presenting greater values of mean dose / V12Gy / V80% / V50% / V10%. (Example: Higher ranks = 8 for VMAT Mean Dose (Gy), indicating 8 VMAT plans received a greater normal brain mean dose value than their Elements MBM counterparts.)

The difference in maximum doses to the OAR was not statistically significant (Table 5). 9 out of 14 OARs identified received a smaller maximum dose on average in the plans generated by the DCAT system, and 13 OARs had a greater number of superior plans in DCAT than in VMAT. The median of the maximum doses to the pituitary was 0.52 Gy (range 0.09–3.04 Gy) for VMAT plans versus 0.26 Gy (range 0.09–2.36 Gy) for DCAT plans. To the left and right inner ear, the median maximum doses were 0.54 Gy and 1.04 Gy for VMAT, compared to 0.59 Gy and 0.42 Gy for DCAT. For the left and right lenses, left and right eye, maximum doses were observed higher in DCAT plans, while that to the optic chiasm was also higher for VMAT plans at 1.33 Gy (range 0.37–3.79 Gy) versus DCAT plans at 0.83 Gy (range 0.30–3.56 Gy).

Dose distribution indices are summarized in Table 6. Differences in mean values show that DCAT plans achieved smaller RTOG CI, higher Paddick CI, and smaller GI on average at 1.24 ± 0.16 , 0.75 ± 0.08 , and 4.00 ± 1.04 , versus VMAT plans at 1.53 ± 0.54 , 0.68 ± 0.14 , and 5.26 ± 2.39 , $p < 0.01$, while VMAT plans achieved lower RTOG HI and ICRU83 HI at 1.23 ± 0.05 and 0.15 ± 0.02 versus DCAT plans at 1.25 ± 0.05 and 0.18 ± 0.02 , $p < 0.01$.

Discussion

The study investigated the dosimetric and radiobiological outcomes of VMAT and DCAT by a clinical comparison of 33 targets recruited from MBM patients. While high-quality treatment plans could be generated using both techniques, significant differences were observed in target coverage, NTCP, dose delivered to the whole brain and OAR, and dose distributions, which should be considered in clinical decision-making. Both techniques fulfilled adequate target coverage and satisfied the oncologist's dose prescription by achieving $> 99.5\%$ of the PTV volume and full coverage ($> 100\%$) of the GTV volume at the 80% isodose prescription. Both techniques prevented the occurrence of hot spots by keeping the near maximum point dose (D2%) in each PTV controlled below 130% as requested. The results show that VMAT provided a larger median near-minimum dose (D98%) of 21.10 Gy at 105.25% of the prescription dose, yet lower D50% and D2%. This suggests that VMAT plans favor a larger isodose cloud with better homogeneity to achieve more extensive target volume coverage but a less favorable dose-target conformity. The finding coincides with Liu et al.²⁸ that VMAT plans favored moderate-to-high isodose metrics while DCAT plans favored low-dose metrics.

OAR	Technique	Median Average Dose (Gy)	Mean Average Dose (Gy)	Range	Superior Plans [†]	2-tailed p-value	Z value
Left Cochlea	VMAT	0.43	0.91	0.06–2.81	5	0.86	−0.18
	DCAT	0.46	0.83	0.06–2.92	6		
Right Cochlea	VMAT	0.77	1.24	0.13–3.16	4	0.33	−0.98
	DCAT	0.41	1.04	0.04–3.15	7		
OAR	Technique	Median Maximum Dose (Gy)	Mean Maximum Dose (Gy)	Range	Superior plans [†]	2-tailed p-value	Z value
Brain Stem	VMAT	2.08	2.42	0.43–6.58	1	0.05	−1.96
	DCAT	1.33	1.96	0.37–5.29	10		
Left Lens	VMAT	0.22	0.43	0.04–1.18	5	0.86	−0.18
	DCAT	0.23	0.52	0.05–2.50	6		
Right Lens	VMAT	0.23	0.35	0.03–0.82	6	0.16	−1.42
	DCAT	0.30	0.52	0.11–1.62	5		
Left Eye	VMAT	0.42	0.84	0.16–2.41	5	1.00	0.00
	DCAT	0.32	0.86	0.26–3.16	6		
Right Eye	VMAT	0.51	0.71	0.22–1.94	5	0.48	−0.71
	DCAT	0.56	0.83	0.18–2.45	6		
Left Inner Ear	VMAT	0.54	1.20	0.20–3.88	5	0.20	−1.27
	DCAT	0.59	1.09	0.07–3.85	6		
Right Inner Ear	VMAT	1.04	1.26	0.19–3.49	6	0.92	−0.10
	DCAT	0.42	1.20	0.07–3.79	5		
Pituitary	VMAT	0.52	0.87	0.09–3.05	3	0.25	−1.16
	DCAT	0.26	0.76	0.09–2.36	8		
Left Optic Nerve	VMAT	0.47	0.86	0.08–2.71	5	0.48	−0.71
	DCAT	0.46	0.76	0.07–2.23	6		
Right Optic Nerve	VMAT	0.53	1.04	0.14–3.92	4	0.21	−1.25
	DCAT	0.41	0.72	0.19–2.05	7		
Optic Chiasm	VMAT	1.33	1.34	0.37–3.79	4	0.21	−1.25
	DCAT	0.83	1.23	0.30–3.56	7		
Spinal Cord	VMAT	0.25	0.75	0.06–2.13	5	1.00	0.00
	DCAT	0.20	0.75	0.03–2.35	6		

Table 5. Mean or maximum doses to the OAR. [†]Superior plans: plans received smaller mean or maximum dose at the given OAR.

	Technique	Mean	Range	SD [‡]	Superior Plans [†]	2-tailed p-value
RTOG CI	VMAT	1.53	1.14–3.47	0.54	10	< 0.01
	DCAT	1.24	0.97–1.60	0.16	20	
Paddick CI	VMAT	0.68	0.45–0.88	0.14	11	< 0.01
	DCAT	0.75	0.59–0.93	0.08	22	
GI	VMAT	5.26	2.60–10.76	2.39	8	< 0.01
	DCAT	4.00	2.45–6.80	1.04	25	
RTOG HI	VMAT	1.23	0.99–1.30	0.05	28	0.05
	DCAT	1.25	1.00–1.32	0.05	4	
ICRU83 HI	VMAT	0.15	0.09–0.20	0.02	29	< 0.01
	DCAT	0.18	0.14–0.21	0.02	4	

Table 6. Dose distribution assessment indices. [†]Superior plans: plans presenting lower RTOG CI, greater Paddick CI, lower GI, lower RTOG HI, or lower ICRU83 HI. [‡]SD: Standard Deviation.

The dosimetric characteristics of VMAT and DCAT can be visualized from a sample plan in Fig. 3 which has a prescription of 20 Gy at 80% isodose line. Comparing the VMAT generated plan (Fig. 3A) against DCAT generated plan (Fig. 3B) shows a more visible dose bridge between individual targets. A wider dose bridge indicates a larger volume of dose spill, so that the normal tissue at the close vicinity of the targets is more likely to be irradiated; The point dose was measured to be 958.2 cGy (VMAT) versus 560.9 cGy (DCAT) at the same location (difference ± 0.1 mm) at the middle of the dose bridges, see Fig. 3. Comparing Fig. 3A(2) and B(2) which contain the cumulative dose volume histograms (cDVH), both VMAT and DCAT saw sharp dose fall-off at PTV and GTV margins with comparably good local control represented by low doses to the normal brain.

Radionecrosis is a crucial risk to consider when planning for individualized SRS treatment⁴⁰. Although Raza²⁵ and Hofmaier²⁶ observed significantly lower V12Gy and better normal tissue sparing in DCAT plans compared to VMAT plans, in our study, the maximum dose and volume of the whole brain receiving 12 Gy (V12Gy) or higher were found to be similar. The UK consensus has identified V12Gy as an important independent predictor of both symptomatic and asymptomatic radionecrosis³¹. According to the similar V12Gy values observed, VMAT and DCAT showed a similar ability to reduce the risk of radionecrosis and to preserve NCF.

Another important indicator of radionecrosis risk was the NTCP outcomes, which were kept below 5% for both VMAT (0.13%, range 0.01–4.39%) and DCAT (0.11%, range 0.02–1.09%), both showing good local control under careful treatment modulation. In line with this finding, the whole brain V12Gy, V10Gy, V8Gy, and V5Gy showed no significant differences between VMAT plans and DCAT plans in this study, although DCAT plans presented with slightly higher median values for all these indices, which was not surprising given its larger volume of the prescription isodose cloud. Therefore, for patients with relatively larger individual targets whose central areas are likely to experience less uniform dose distribution, VMAT might be clinically effective in achieving adequate dose coverage at GTV margins and in better preventing the occurrence of hot spots as the target gets larger, although the OAR maximum dose may be potentially compromised. Nevertheless, dynamic trajectory radiotherapy (DTRT) has been developed as an VMAT extension by allowing non-coplanar beam delivery with dynamic table and collimator rotations⁴¹, DTRT has improved the dosimetric features and has shown promising results in reducing OAR dose and NTCP compared to VMAT⁴². Future studies are needed to further compare the clinical performance between DTRT and DCAT.

It should also be noted that for any single case, the absolute values of predicted NTCP outcomes may not be reliable, but it is the difference in NTCP that can provide useful information when alternate treatment plans are compared⁴³. The uncertainty in the absolute value of NTCP is thus inevitable. One limitation of our NTCP computation is the use of published parameter values. Although these parameter values were highly appreciated, any variation in these values can lead to changes in the NTCP results calculated. For instance, the tissue-specific parameter $\alpha = 9$ was obtained from the empirical dose-volume fitting by Emami et al.³⁷; however, analogous data can also be obtained from an individual institutional practice⁴⁴. Thus, for a given institution, using NTCP model parameters based on the calibration of a selected model against average clinical outcomes can potentially yield more accurate NTCP values reflecting situational situations. For a clinic that would like to include NTCP in radionecrosis evaluation, the implementation of NTCP algorithms is another option, such as Philips Pinnacle and Varian Eclipse embedded with the Lyman model and Poisson model for NTCP/TCP⁴⁵.

Previous comparison studies have reported different results regarding the conformity of VMAT and DCAT techniques. Such discrepancies may be due to differences in plan optimization when processing lesions of different sizes and shapes. In this study, VMAT treated plans presented with more uniform dose distribution indicated by a significantly smaller RTOG HI and ICRU83 HI, preventing the hot spots occurring. On the other hand, DCAT achieved superior conformity with a smaller average RTOG CI at 1.24 ± 0.16 compared to VMAT (RTOG CI 1.53 ± 0.54), which was further supported by the higher mean Paddick CI (0.75 ± 0.08) observed in the DCAT plans than in VMAT plans (0.68 ± 0.14). For VMAT plans, we observed that Paddick CI decreased as the target volume decreased, as shown in Fig. 4, which is likely to be caused by over-dosage, especially for smaller targets where the high-dose spills appeared more prominent. A study comparing VMAT against CK showed that although VMAT presented with better treatment efficiency than CK in treating MBM, its conformity was lower owing to the greater PTV margin⁴⁶. Similar conclusions were also drawn in a dosimetric comparison

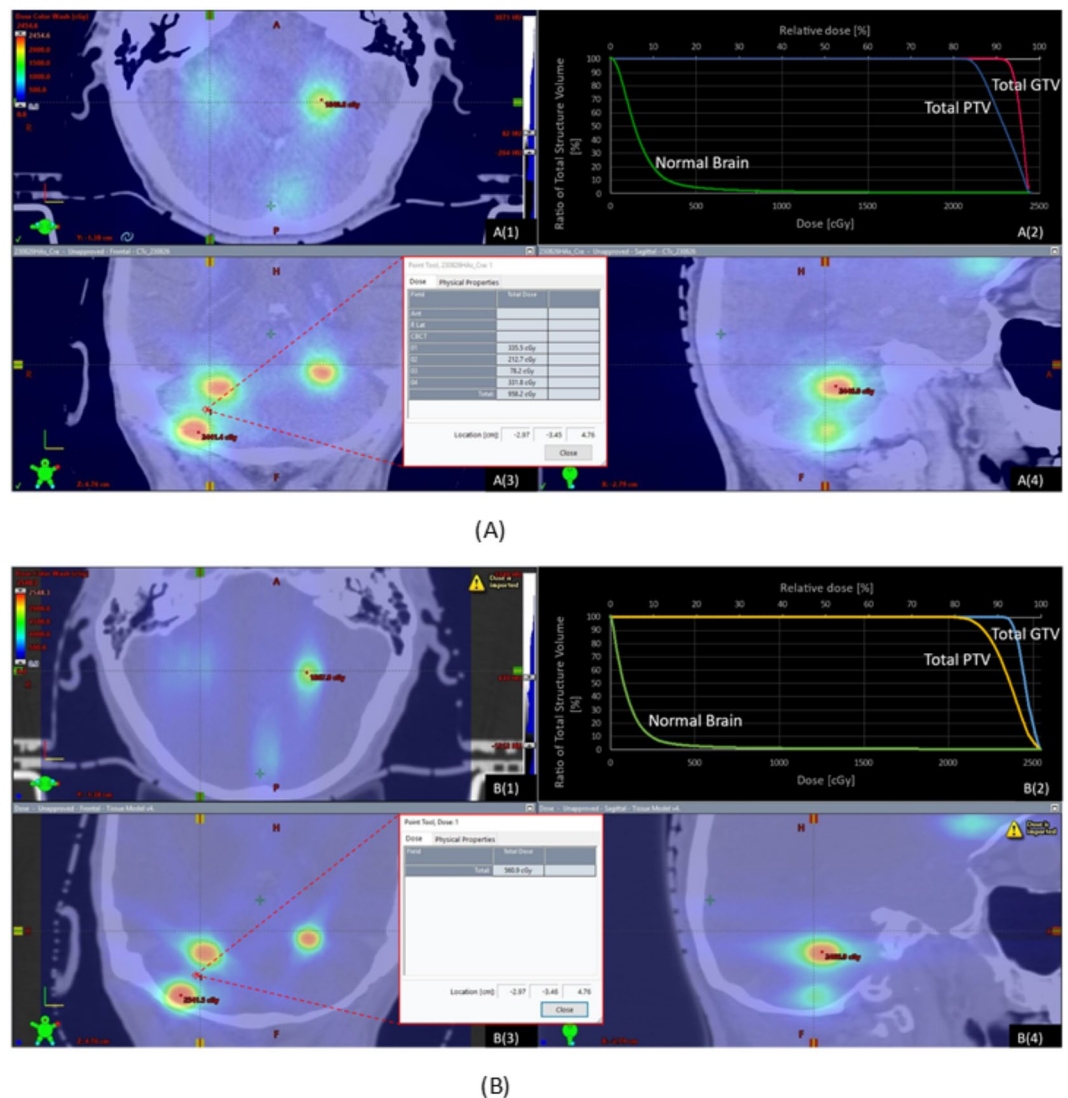


Fig. 3. Dose distributions of a case with a prescription of 20 Gy at 80% isodose line. **(A)** Dose distribution of the VMAT plan. A(1): Transversal, Y=-1.38 cm; A(2): cDVH of total PTV, total GTV, and Normal Brain; A(3): Frontal, Z=4.76 cm; A(4): Sagittal, X=-2.79 cm. The point dose at the middle of the dose bridge (location X=-2.97 cm, Y=-3.45 cm, Z=4.76 cm) was 958.2 cGy. **(B)** Dose distribution of the DCAT plan. B(1): Transversal, Y=-1.38 cm; B(2): cDVH of total PTV, total GTV, and Normal Brain; B(3): Frontal, Z=4.76 cm; B(4): Sagittal, X=-2.79 cm. The point dose at the middle of the dose bridge (location X=-2.97 cm, Y=-3.46 cm, Z=4.76 cm) was 560.9 cGy.

between GK and VMAT⁴⁷. Our finding also suggested that DCAT plans achieved a smaller GI of 4.00 ± 1.04 compared to VMAT plans (5.26 ± 2.39). Since the smaller the GI the sharper the dose fall-off, an increase in GI value is associated with the risk of normal tissue dose. In this way, regions of tissue outside the targets of DCAT-generated plans are less likely to experience NCF decline, consistent with previous studies^{26,27}.

According to Figs. 4, 5 and 6, DCAT plans maintained smaller variations in dose distribution indices despite the variation in target sizes, indicating that the dose distributions of DCAT plans were less likely to be affected by the decline in target volumes. Narayanasamy et al.²⁹ noted that DCAT primarily uses a dynamic conformal arc approach for dose optimization, producing MLC segments typically of the same size as the treated tumors, resulting in superior planning conformity compared to VMAT. In clinical practice, target volumes as small as 1 cc are not uncommon. Considering the results of GI and CI, it is recommended that patients with small individual PTV volumes (< 1 cc) may benefit from DCAT treatment to reduce normal tissue dose.

The limitations of this study include its single-institution design, which results in a relatively small sample size that may not accurately reflect the situation of a larger patient population treated at various clinical centers. Additionally, most of the PTV included in this study consisted of low volumes and high sphericity, thus the influence of PTV size and shape on the performance of DCAT and VMAT may not be addressed adequately. Future multi-institutional studies using larger sample sizes, different energy profiles, and diverse target sphericity are needed to verify the results.

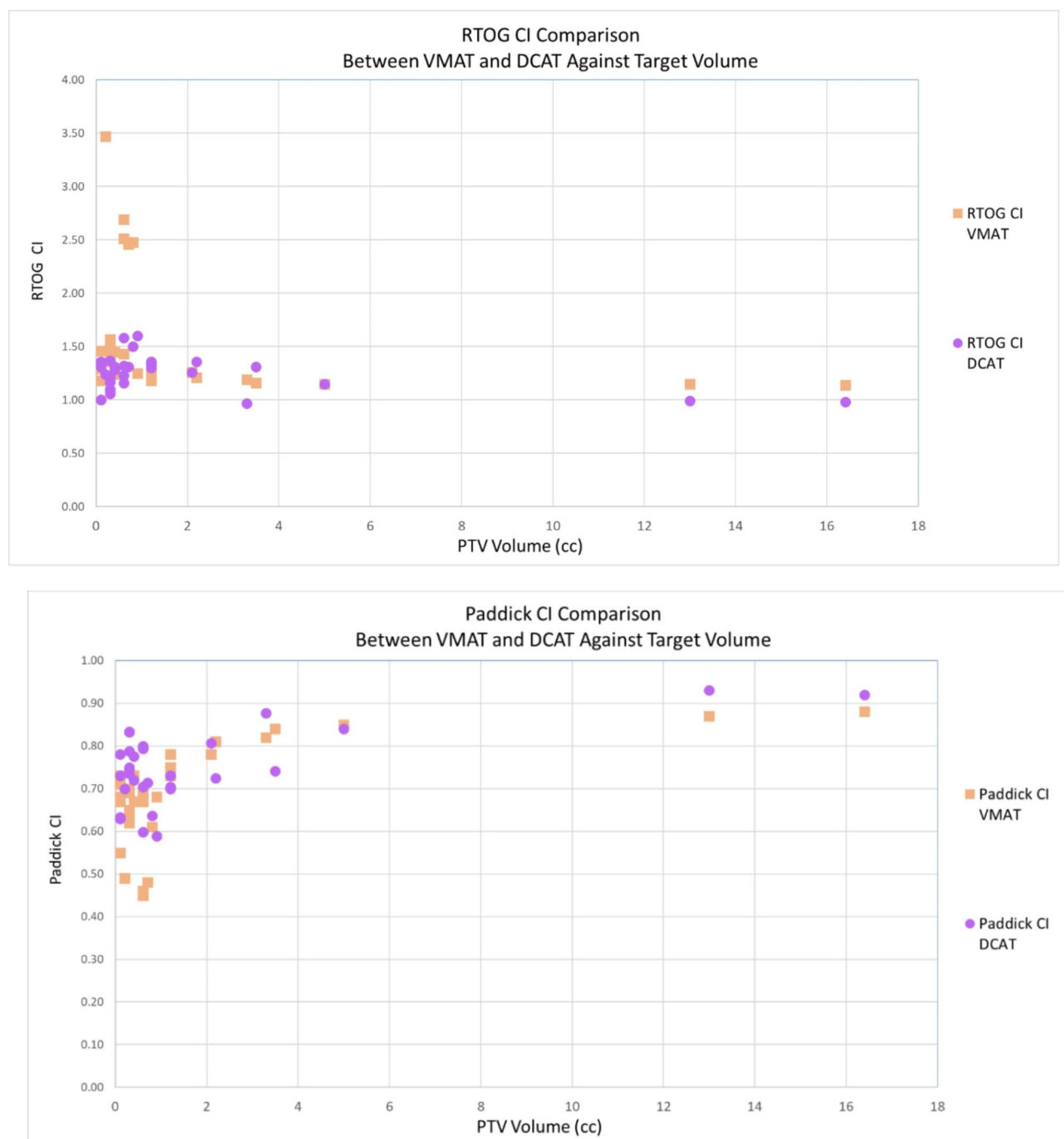


Fig. 4. Conformity Indices (RTOG CI and Paddick CI) Against PTV (cc).

Conclusion

This clinical comparison study compared the treatment plan quality of VMAT and DCAT techniques in terms of target coverage, NTCP, and dose distribution, providing insights into the dosimetric and radiobiological outcomes of the two techniques. To protect NCF and improve QoF after SRS in an individualized treatment plan, it is important to consider these differences. Both techniques achieved remarkably low NTCP under clinical settings. HA plans tended to have a higher target dose profile with more adequate target coverage but with a larger volume of high, medium, and low dose spills, and better dose homogeneity. Meanwhile, Elements MBM plans exhibited better beam conformity and steeper dose gradient, and the plan quality was less susceptible to target size variations. We recommend for patients with small PTV volumes less than 1 cc, DCAT might be a better clinical option while VMAT should be considered for large intracranial targets where hot spots could easily appear. In general, the results showed that both VMAT and DCAT were able to generate high-quality SRS plans under the careful treatment modulation by radiation oncologists and medical physicists.

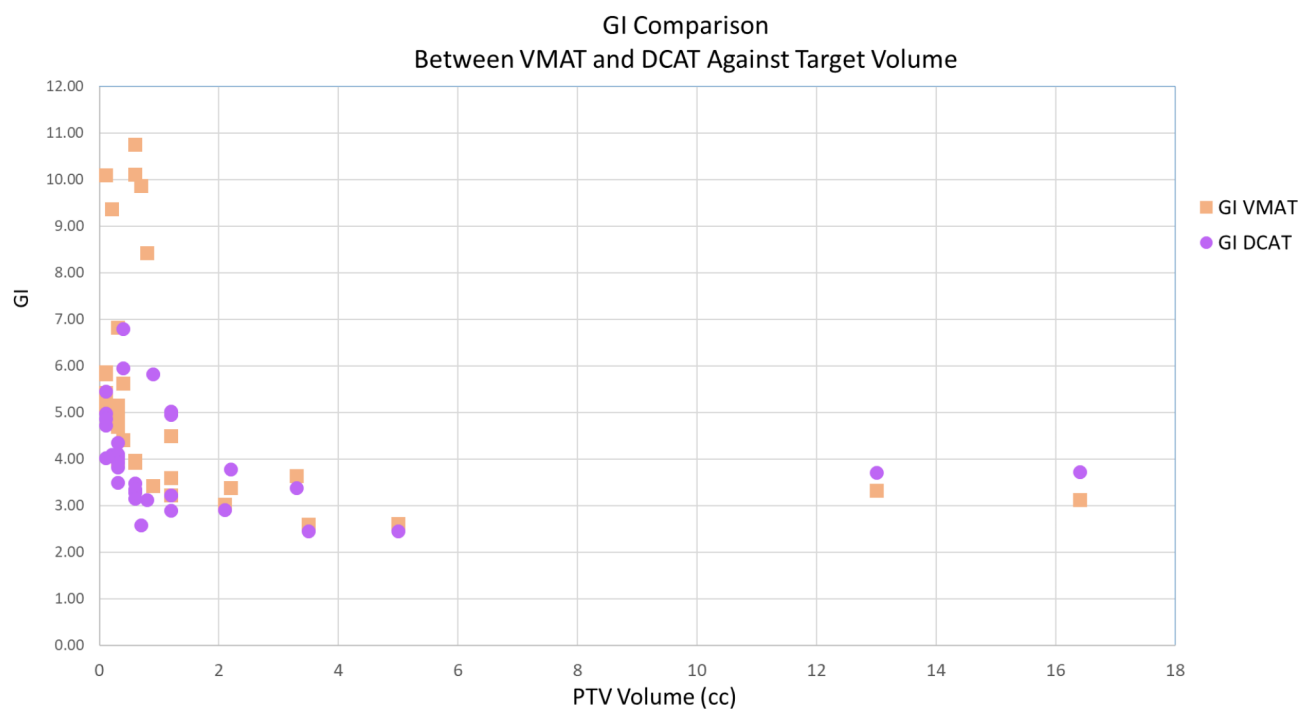


Fig. 5. Gradient Index Against PTV (cc).

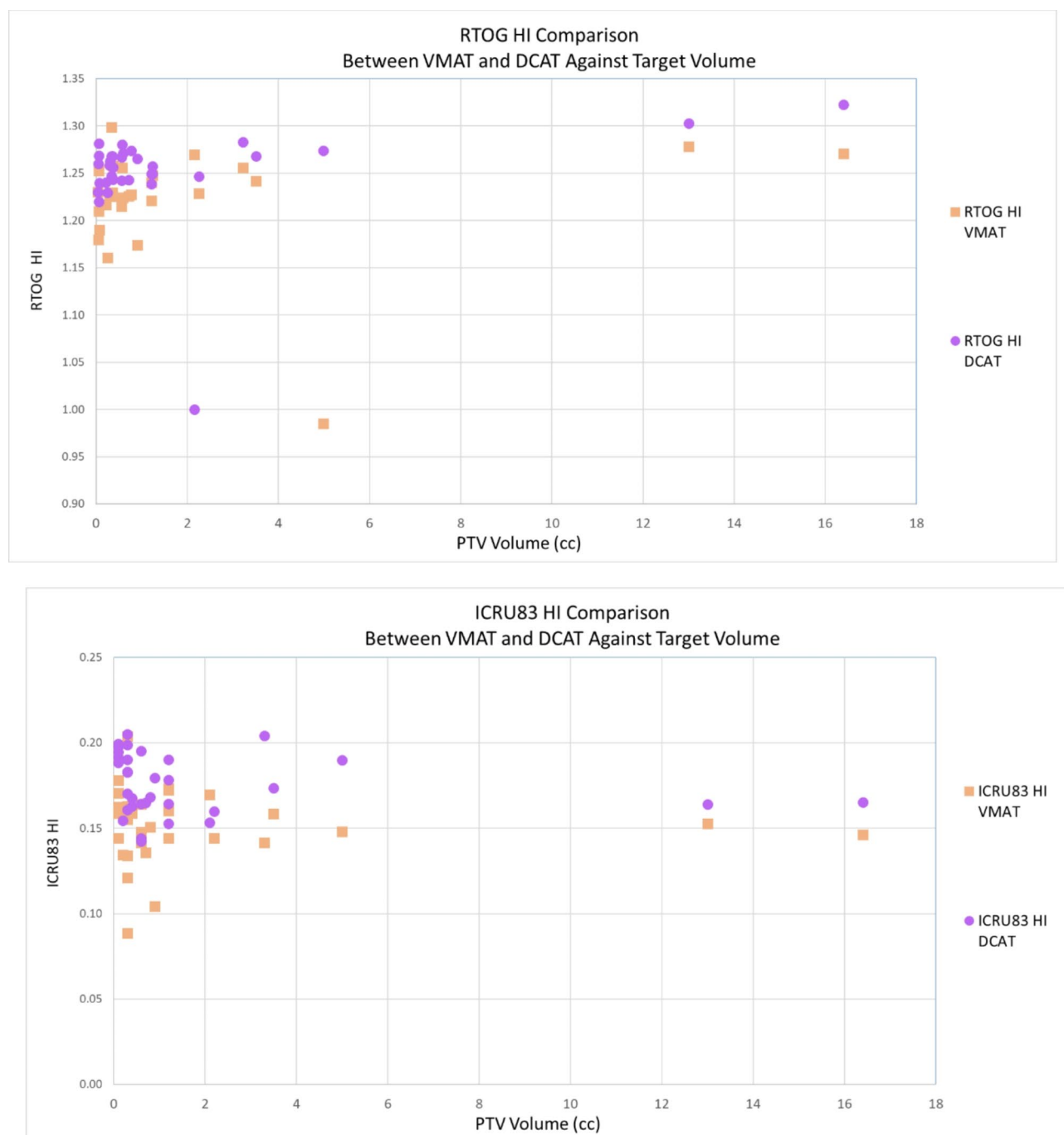


Fig. 6. Homogeneity Indices (RTOG HI and ICRU83 HI) Against PTV (cc).

Data availability

A summary of data used to support the findings is included in the article. Patient specific data were collected from the Union Oncology Centre, Union Hospital approved by the ethics committee and is available upon reasonable request to the corresponding author Harry Chi-yuen CHENG chenghcy@union.org.

Received: 16 October 2024; Accepted: 7 March 2025

Published online: 17 March 2025

References

1. Eichler, A. F. et al. The biology of brain metastases—translation to new therapies. *Nat. Rev. Clin. Oncol.* **8**(6), 344–356 (2011).
2. Barnholtz-Sloan, J. S. et al. Incidence proportions of brain metastases in patients diagnosed (1973 to 2001) in the metropolitan Detroit Cancer surveillance system. *J. Clin. Oncol.* **22**(14), 2865–2872 (2004).

3. Alongi, F., Fiorentino, A., Navarra, P., Bello, L. & Scorsetti, M. Stereotactic radiosurgery for patients with brain metastases. *Lancet Oncol.* **15**(7), e246–247 (2014).
4. Gondi, V. et al. Radiation therapy for brain metastases: An ASTRO clinical practice guideline. *Pract. Radiat. Oncol.* **12**(4), 265–282 (2022).
5. Patil, C. G. et al. Whole brain radiation therapy (WBRT) alone versus WBRT and radiosurgery for the treatment of brain metastases. *Cochrane Database Syst. Rev.* **9** (2017).
6. Limon, D. et al. Single fraction stereotactic radiosurgery for multiple brain metastases. *Adv. Radiat. Oncol.* **2**(4), 555–563 (2017).
7. Lau, S. K. M. et al. Single-Isocenter frameless volumetric modulated Arc radiosurgery for multiple intracranial metastases. *Neurosurgery* **77**(2), 233–240 (2015).
8. Murai, T. et al. Comparison of multileaf collimator and conventional circular collimator systems in cyberknife stereotactic radiotherapy. *J. Radiat. Res.* **58**(5), 693–700 (2017).
9. Bertholet, J. et al. Organs-at-risk dose and [internet]ormal [internet]issue complication probability with dynamic [internet]rajectory [internet]adiotherapy (DTRT) for head and [internet]eck cancer. *Radiation Oncol.* **20** (2024). 95:110237–110237.
10. Loebner, H. A. et al. Robustness analysis of dynamic trajectory radiotherapy and volumetric modulated Arc therapy plans for head and neck cancer. *Phys. [Internet]aging Radiation Oncol. [Internet]* **30**, 100586 (2024).
11. Kim, C. et al. Evaluation of the deliverability of dynamic conformal Arc therapy (DCAT) by gantry wobble and its influence on dose. *Sci. Rep.* **14**(1), 7134 (2024).
12. Ladbury, C. et al. Stereotactic radiosurgery in the management of brain metastases: A Case-Based radiosurgery society (RSS) practice guideline: Brain metastasis SRS RSS practice guideline. *Adv. Radiation Oncol.* **9**(3), 101402 (2023).
13. Vergalasova, I. et al. Multi-Institutional dosimetric evaluation of modern day stereotactic radiosurgery (SRS) treatment options for multiple brain metastases. *Front. Oncol.* **9**. (2019).
14. Tas, B. et al. Heterogeneity index, and size of metastasis correlations for LINAC-Based stereotactic radiosurgery/radiation therapy. *Int. J. Radiat. Oncol. Biol. Phys.* **99**(2), E727 (2017).
15. Minniti, G. et al. Stereotactic radiosurgery for brain metastases: analysis of outcome and risk of brain radionecrosis. *Radiat. Oncol.* **6**(48). (2011).
16. Chin, L. S., Ma, L. & DiBiase, S. Radiation necrosis following gamma knife surgery: A case-controlled comparison of treatment parameters and long-term clinical follow up. *J. Neurosurg.* **94**(6), 899–904 (2001).
17. Korytko, T. et al. 12 Gy gamma knife radiosurgical volume is a predictor for radiation necrosis in non-AVM intracranial tumors. *Int. J. Radiat. Oncol. Biol. Phys.* **64**(2), 419–424 (2006).
18. Monje, M. L., Mizumatsu, S., Fike, J. R. & Palmer, T. D. Irradiation induces neural precursor-cell dysfunction. *Nat. Med.* **8**(9), 955–962 (2002).
19. Milano, M. T. et al. Single- and multifraction stereotactic radiosurgery dose/volume tolerances of the brain. *Int. J. Radiat. Oncol. Biol. Phys.* **110**(1), 68–86 (2021).
20. Milano, M. T. et al. Single- and Multi-Fraction stereotactic radiosurgery dose tolerances of the optic pathways. *Int. J. Radiat. Oncol. Biol. Phys.* **110**(1), 87–99 (2021).
21. Redmond, K. J. et al. Tumor control probability of radiosurgery and fractionated stereotactic radiosurgery for brain metastases. *Int. J. Radiat. Oncol. Biol. Phys.* **110**(1), 53–67 (2021).
22. Marks, L. B. et al. The use of normal tissue complication probability (NTCP) models in the clinic. *Int. J. Radiat. Oncol. Biol. Phys.* **76**(3), S10–S19 (2010).
23. Niemierko, A. Reporting and analyzing dose distributions: A concept of equivalent uniform dose. *Med. Phys.* **24**(1), 103–110 (1997).
24. Niemierko, A. & Goitein, M. Modeling of normal tissue response to radiation: The critical volume model. *Int. J. Radiat. Oncol. Biol. Phys.* **25**(1), 135–145 (1993).
25. Raza, G. H. et al. Single-isocenter multiple-target stereotactic radiosurgery for multiple brain metastases: Dosimetric evaluation of two automated treatment planning systems. *Radiat. Oncol.* **17**(1). (2022).
26. Hofmaier, J. et al. Single isocenter stereotactic radiosurgery for patients with multiple brain metastases: Dosimetric comparison of VMAT and a dedicated DCAT planning tool. *Radiat. Oncol.* **14**(1). (2019).
27. Gevaert, T. et al. Evaluation of a dedicated brain metastases treatment planning optimization for radiosurgery: A new treatment paradigm? *Radiat. Oncol.* **11**(1). (2016).
28. Liu, H. et al. Interinstitutional plan quality assessment of 2 Linac-Based, Single-Isocenter, multiple metastasis radiosurgery techniques. *Adv. Radiation Oncol.* **5**(5), 1051–1060 (2020).
29. Narayanasamy, G. et al. A systematic analysis of 2 monoisocentric techniques for the treatment of multiple brain metastases. *Technol. Cancer Res. Treat.* **16**(5), 639–644 (2016).
30. Ruggieri, R. et al. Linac-based radiosurgery for multiple brain metastases: Comparison between two mono-isocenter techniques with multiple non-coplanar arcs. *Radiation Oncol.* **132**, 70–78 (2019).
31. Diez, P. et al. UK 2022 consensus on normal tissue Dose-Volume constraints for oligometastatic, primary lung and hepatocellular carcinoma stereotactic ablative radiotherapy. *Clin. Oncol.* **34**(5), 288–300 (2022).
32. Paddick, I. A simple scoring ratio to index the conformity of radiosurgical treatment plans. Technical note. *J. Neurosurg.* **93**(3), 219–222 (2000).
33. Simon, M., Papp, J., Csiki, E. & Kovács, Á. Plan quality assessment of fractionated stereotactic radiotherapy treatment plans in patients with brain metastases. *Front. Oncol.* **12** (2022).
34. Reynolds, T. A., Jensen, A. R., Bellairs, E. E. & Ozer, M. Dose gradient index for stereotactic radiosurgery/radiation therapy. *Int. J. Radiat. Oncol. Biol. Phys.* **106**(3), 604–611 (2020).
35. Kataria, T., Sharma, K., Subramani, V., Karthick, K. P. & Bisht, S. S. Homogeneity index: an objective tool for assessment of conformal radiation treatments. *J. Med. Phys.* **37**(4), 207–213 (2012).
36. Niemierko, A. A free program for calculating EUD-based NTCP and TCP in external beam radiotherapy. *Eur. J. Med. Phys.* **23**(3–4), 115–125 (2007).
37. Emami, B. et al. Tolerance of normal tissue to therapeutic irradiation. *Int. J. Radiat. Oncol. Biol. Phys.* **21**(1), 109–122 (1991).
38. Burman, C., Kutcher, G. J., Emami, B. & Goitein, M. Fitting of normal tissue tolerance data to an analytic function. *Int. J. Radiat. Oncol. Biol. Phys.* **21**(1), 123–135 (1991).
39. Okunieff, P., Morgan, D., Niemierko, A. & Suit, H. Radiation dose-response of human tumors. *Int. J. Radiat. Oncol. Biol. Phys.* **32**(4), 1227–1237 (1995).
40. Minniti, G. et al. Initial experience with Single-Isocenter radiosurgery to target multiple brain metastases using an automated treatment planning software: Clinical outcomes and optimal target volume margins strategy. *Adv. Radiation Oncol.* **5**(5), 856–864 (2020).
41. Fix, M. K. et al. Part 1: Optimization and evaluation of dynamic trajectory radiotherapy. *Med. Phys.* **45**(9), 4201–4212 (2018).
42. Loebner, H. A. et al. Impact of the gradient in gantry-table rotation on dynamic trajectory radiotherapy plan quality. *Med. Phys.* **50**(11), 7104–7117 (2023).
43. Wu, Q. et al. Intensity-modulated radiotherapy optimization with gEUD-guided dose volume objectives. *Phys. Med. Biol.* **48**(3), 279–291 (2003).
44. Lawrence, Y. R. et al. Radiation Dose–Volume effects in the brain. *Int. J. Radiat. Oncol. Biol. Phys.* **76**(3), S20–S27 (2010).

45. Allen, X. L. et al. The use and QA of biologically related models for treatment planning: Short report of the TG-166 of the therapy physics committee of the AAPM. *Med. Phys.* **39**(3), 1386–1409 (2012).
46. Shafie, R. A. E. et al. Single-Isocenter volumetric modulated Arc therapy vs. CyberKnife M6 for the stereotactic radiosurgery of multiple brain metastases. *Front. Oncol.* **10** (2020).
47. Potrebko, P. S. et al. GammaKnife versus VMAT radiosurgery plan quality for many brain metastases. *J. Appl. Clin. Med. Phys.* **19**(6), 159–165 (2018).

Author contributions

Chen-jun JIANG and Harry Chi-yuen CHENG designed and drafted the manuscript. Yick-wing HO, Ka-hei LO and Chen-jun JIANG oversaw data collection and analysis. Chun-Ran ZHU and Yeow-Yuen LU participated in literature review. Harry Chi-yuen CHENG monitored the quality of this study. All authors reviewed and approved the manuscript.

Declarations

Competing interests

The authors declare no competing interests.

Additional information

Supplementary Information The online version contains supplementary material available at <https://doi.org/10.1038/s41598-025-93502-7>.

Correspondence and requests for materials should be addressed to C.-J.J., C.-R.Z. or H.C.-Y.C.

Reprints and permissions information is available at www.nature.com/reprints.

Publisher's note Springer Nature remains neutral with regard to jurisdictional claims in published maps and institutional affiliations.

Open Access This article is licensed under a Creative Commons Attribution-NonCommercial-NoDerivatives 4.0 International License, which permits any non-commercial use, sharing, distribution and reproduction in any medium or format, as long as you give appropriate credit to the original author(s) and the source, provide a link to the Creative Commons licence, and indicate if you modified the licensed material. You do not have permission under this licence to share adapted material derived from this article or parts of it. The images or other third party material in this article are included in the article's Creative Commons licence, unless indicated otherwise in a credit line to the material. If material is not included in the article's Creative Commons licence and your intended use is not permitted by statutory regulation or exceeds the permitted use, you will need to obtain permission directly from the copyright holder. To view a copy of this licence, visit <http://creativecommons.org/licenses/by-nc-nd/4.0/>.

© The Author(s) 2025